ARTICLE

Investigation of Ultrafast Excited-State Dynamics of 3-Furfural†

Wenping Wu[a,b], Yuhuan Tian[a,b], Zhigang He[a], Dongyuan Yang[a*], Guorong Wu[a*], Xueming Yang[a,c]

a. State Key Laboratory of Molecular Reaction Dynamics, Dalian Institute of Chemical Physics, Dalian 116023, China
b. University of Chinese Academy of Sciences, Beijing 100049, China
c. Department of Chemistry, College of Science, Southern University of Science and Technology, Shenzhen 518055, China

(Dated: Received on July 30, 2024; Accepted on September 4, 2024)

3-Furfural($C_5H_4O_2$) is a furan(C_4H_4O) derivative compound formed by replacing the hydrogen (H) atom at the ring 3-position with the aldehyde (CHO) group substituent. In this work, we intend to investigate the ultrafast decay dynamics of electronically excited 3-furfural using the femtosecond time-resolved photoelectron imaging technique. At pump wavelengths of 259.5, 238.6 and 218.3 nm, two alternative decay mechanisms for the $S_2(^1\pi\pi^*)$ state are tentatively proposed and discussed. Specifically, we prefer to suggest that a fraction of the initially prepared wavepacket in the $S_2(^1\pi\pi^*)$ state is likely to undergo the subpicosecond relaxation via the $S_1(^1n\pi^*)$ state. Presumably the lower lying $T_2(^3\pi\pi^*)$ state is subsequently populated on a ~4 ps timescale via intersystem crossing from the minimum of the $S_1(^1n\pi^*)$ state surface. The relaxation of the $T_2(^3\pi\pi^*)$ state is sensitive to its vibrational excess energy and the value of its lifetime is 1.6±0.2 ns, 280±30 ps and 50±10 ps for pump wavelengths of 259.5, 238.6 and 218.3 nm, respectively.

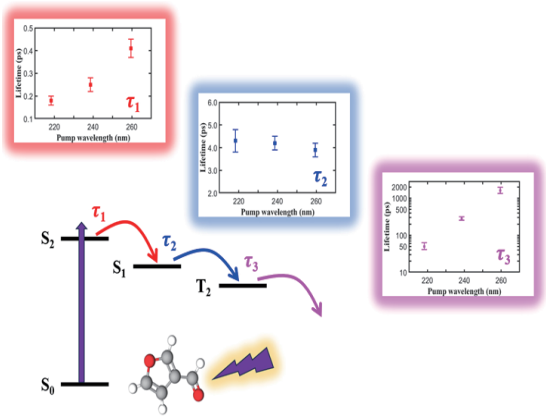

Key words: Femtosecond time-resolved, Photoelectron imaging, Ultrafast decay dynamics

I. INTRODUCTION

The photochemical and photophysical behaviors of small isolated heteroaromatic molecules have been the subject of extensive studies [1, 2]. For example, pyrrole and furan are two prototypical five-membered heteroaromatic molecules containing one heteroatom. The investigation on the excited-state dynamics of such ideal model molecules promotes the understanding of electronic structure and photochemistry of larger molecular systems [3–5]. Previously, we have investigated the ultraviolet-induced excited-state decay dynamics of pyrrole [6] and a series of its substituted derivatives [7–11]. The substitution effects on the excited-state dynamics of pyrrole are better understood. For the bare furan, the excited-state dynamics has been studied both experimentally and theoretically [4, 5, 12–19] over the past few decades. A deeper understanding of ultrafast internal conversion of furan upon ultraviolet (UV) excitation at 200 nm was achieved by using extreme ultraviolet (EUV) time-resolved photoelectron spectroscopy (TRPES) with a time resolution of 15 fs [5]. In recent

† Part of Special Issue "In Memory of Prof. Xingxiao Ma on the occasion of his 90th Anniversary".
* Authors to whom correspondence should be addressed. E-mail: yangdy@dicp.ac.cn, wugr@dicp.ac.cn

years, some studies have focused on the photochemical properties of substituted derivatives of furan [20–24]. Specifically, 3-furfural (other names, *e.g.*, 3-furaldehyde, 3-formylfuran or furan-3-carbaldehyde) is one of the aldehyde derivatives of furan. Substituent effects on the relaxation dynamics of furan, furfural, and 3-furfural have been reported by de Vivie-Riedle and coworkers [21]. According to their investigation, both experimental and theoretical results showed that the relaxation dynamics is slowed down due to the influence of an aldehyde group substituted at its 2- or 3-position. Moreover, compared with the relaxation dynamics of furan, an additional deactivation pathway involving the $^1n_O\pi^*$ state opens for the $S_2(^1\pi\pi^*)$ state in the cases of furfural and 3-furfural.

In this paper, we focus solely on 3-furfural and present a femtosecond time-resolved photoelectron imaging (fs-TRPEI) study of the $S_2(^1\pi\pi^*)$ state decay dynamics. Based on a detailed analysis of the experimental TRPES data, a comprehensive picture is proposed for the ultrafast decay dynamics of electronically excited 3-furfural. It is worth to be mentioned that 3-furfural can display two different conformations in the ground state, named the *trans* and *cis* conformers. The *trans* form is suggested to be more stable than the *cis* form by 4.86 kJ/mol in the gas phase [25, 26]. Thus, we assume that the *trans* configuration of 3-furfural is in the majority under our supersonic jet-cooled molecular beam conditions (*trans*:*cis* is about 8:1 in ratio according to a previous study of the rotational spectrum of 3-furfural in a supersonic jet [26]). The conformer-specific excited-state dynamics is out of the scope of the current study due to the intrinsic broad spectral bandwidth of the femtosecond pump laser pulses and will not be discussed here.

II. EXPERIMENTAL METHODS

The 3-furfural sample with a stated purity of ≥98% was purchased from Aladdin and used without further purification in all aspects of the current study. The UV absorption spectrum of 3-furfural under saturated vapor conditions at room temperature was recorded on a commercial UV-Vis-NIR spectrometer (Agilent, Cary 5000). The TRPEI experiment was carried out on a homemade velocity map imaging (VMI) spectrometer [27]. The experimental methods have been previously described in detail elsewhere [28–31] and only a few of the key features are mentioned here. The vapor of the liquid 3-furfural sample was mixed with ~4 bar of helium carrier gas and expanded supersonically into a high vacuum source chamber via a 1 kHz Even-Lavie valve. The sample was heated with a valve temperature of ~45 °C throughout the experiment. The seeded 3-furfural molecular beam entered into the interaction chamber of the VMI spectrometer through a 1 mm skimmer.

The pump and probe laser pulses were generated from a femtosecond laser system consisting primarily of a fully integrated 1 kHz Ti:sapphire oscillator-regenerative amplifier (Coherent, Libra-HE) and two commercial optical parametric amplifiers (Coherent, OPerA Solo). The pump laser pulses of 259.5, 238.6 and 218.3 nm (0.1-0.3 μJ per pulse) were employed and the probe wavelength was chosen at 403.7 nm (~4.2 μJ per pulse) in the current experiment. The bandwidth of the pump laser pulses (full width at half maximum (FWHM) of the spectrum) of 259.5, 238.6 and 218.3 nm were ~334, ~280 and ~200 cm^{-1}, respectively, and ~217 cm^{-1} for the probe laser pulse of 403.7 nm. The pump and probe laser pulses were combined collinearly on a dichroic mirror without further compression, and then focused using a calcium fluoride lens (typically $f/75$ for the pump and $f/60$ for the probe laser beam) into the interaction region of the VMI spectrometer to intersect the seeded 3-furfural molecular beam. The supersonic jet-cooled 3-furfural molecules were excited by one-photon absorption, whereupon the delayed probe laser pulse of 403.7 nm produced photoelectrons via two-photon ionization.

The polarization direction of all pump and probe laser pulses was parallel to the microchannel plate (MCP)/phosphor screen detector. The 2D photoelectron images were recorded using the computer-controlled camera and transferred to 3D distributions using the pBasex Abel inversion method [32]. The delay-dependent photoelectron 3D distributions were further integrated along the recoiling angle to derive the TRPES spectra. The pump-probe time delays were scanned back and forth multiple times to minimize any small hysteresis effects, and the effects caused by the fluctuations and drifts in molecular beam intensity, laser pulse energy and pointing, *etc.* Electron kinetic energy calibration was performed using multiphoton ionization of xenon atoms [27]. The two-color (1+2′) nonresonant ionization of nitric oxide served to determine the time-zero and the cross-correlation (*i.e.*, instrumental response function (IRF)) between the pump and

DOI: 10.1063/1674-0068/cjcp2407099

probe laser pulses. The (1+2') IRFs were measured to be 130±10 fs (FWHM) based on the approximation that both the pump and probe laser pulses have a Gaussian profile. It was carefully checked that there were negligible 3-furfural clusters presented under our molecular beam conditions.

III. RESULTS AND DISCUSSION

A. The UV absorption spectrum

The UV absorption spectrum of 3-furfural was reported in a previous study [21]. Here, the UV absorption spectrum of vapor-phase 3-furfural molecules is shown in FIG. 1(a). The main feature of this spectrum is a broad and structureless absorption band which starts from ~270 nm. In the case of 3-furfural, it has been well known that the UV absorption cross sections between 290 and 380 nm are less than the order of magnitude of ~1×10^{-19} cm^2·$molecule^{-1}$ [33]. This first absorption band is assigned to the transition to the $S_1(1^1n_o\pi^*)$ state and too weak to be recorded in our measurement of vapor-phase absorption spectrum of 3-furfural. Therefore, it is straightforward to assign the broad absorption band centered around ~238 nm to the transition to the first optically bright $^1\pi\pi^*$ state (S_2 at the Franck-Condon geometry). For deeper excitation wavelengths of <220 nm, the next absorption band starts to appear strongly, resulting in an obvious rising of the overall absorption spectrum. The $S_3(2^1\pi\pi^*)$ state should mainly contribute to this stronger absorption band. Based on the result of a previous theoretical calculation [25], the $S_1(1^1n_o\pi^*)$, $S_2(1^1\pi\pi^*)$ and $S_3(2^1\pi\pi^*)$ states of 3-furfural have different values of the oscillator strength, which are 0.0002, 0.0574 and 0.1524 respectively in the case of *trans* conformer, together with 3.91, 4.92 and 6.01 eV vertical excitation energies. This information supports the above assignment of the absorption bands in a wavelength range of 210–380 nm and is also consistent with the result of another calculation [21].

B. The analysis of TRPES spectra

The pump wavelengths employed in the current time-resolved experiment are 259.5, 238.6 and 218.3 nm, the spectra of which are plotted in FIG. 1(b). The TRPES spectra of 3-furfural at 259.5, 238.6 and 218.3 nm after subtracting the background photoelectrons generated from single-color multiphoton ionization are shown in FIG. 2 (a), (b) and (c), respectively. Note that a combi-

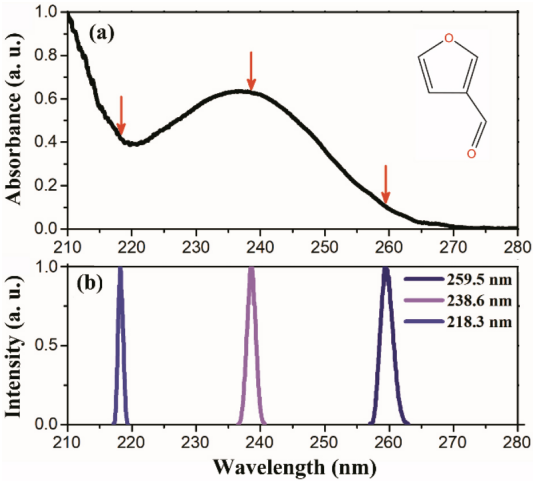

FIG. 1 (a) Room-temperature UV absorption spectrum of 3-furfural vapor. The red arrows indicate the pump wavelengths used in the current experiment. (b) Spectra of the 259.5, 238.6 and 218.3 nm pump wavelengths.

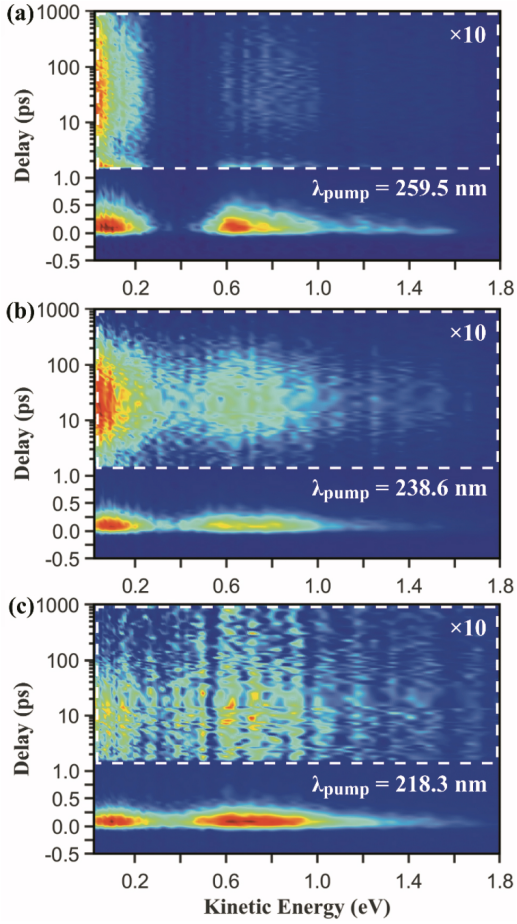

FIG. 2 (a) TRPES spectrum of 3-furfural at pump wavelength of 259.5 nm. A portion of it is scaled up by a factor of 10 for a better presentation. The background photoelectrons generated from single-color multiphoton ionization have been subtracted. Note that a combination of linear (≤1 ps) and logarithmic (≥1 ps) scales is used in the ordinate. (b) and (c) Same as (a), but at pump wavelength of 238.6 and 218.3 nm.

DOI: 10.1063/1674-0068/cjcp2407099

nation of linear (≤1 ps) and logarithmic (≥1 ps) scales is used along the time delay coordinate. At 259.5 and 238.6 nm pump wavelengths, the $S_2(^1\pi\pi^*)$ state of 3-furfural is initially excited according to the assignment of the absorption spectrum. In FIG. 2, the photoelectron spectra at delays of<1 ps share large similarities, dominated by a diffuse and broad distribution over the whole kinetic energy range below 1.8 eV. Both spectra have several peak positions around similar kinetic energies. It should be pointed out that the use of (1+2') ionization in TRPES measurements is likely to involve the resonance with Rydberg state(s) at the (1+1') two-photon excitation energy [34]. Therefore, we do not provide a quantitative analysis of the photoelectron kinetic energy distributions. By visual inspection, the time scale of the dynamics is of hundreds of femtoseconds. At long delay times (>1 ps), a delayed rise of the photoelectron signal can be observed and should be partly associated with the ionization of a subsequently populated lower lying electronic state. The intensity of this delayed rise signal is about one order of magnitude smaller than that of the subpicosecond decay at short delay times. The overall photoelectron kinetic energy distributions in these two delay ranges have some subtle differences in the relative intensity of each peak.

In order to extract more detailed information, a 2D global least-squares method was employed to simultaneously fit TRPES data at all time delays and photoelectron kinetic energies. The kinetic model used can be expressed as the following equation:

$$S(t,\varepsilon_k) = \mathrm{DAS}_0(\varepsilon_k) \times \mathrm{IRF} + \sum_{i=1}^{3} \mathrm{DAS}_i(\varepsilon_k) \times \left\{ \left[\exp\left(-\frac{t}{\tau_i}\right) \times H(t) \right] \otimes \mathrm{IRF} \right\} \quad (1)$$

Here, $S(t,\varepsilon_k)$ represents the 2D TRPES spectrum, while t and ε_k are the pump-probe time delay and the kinetic energy of the emitted photoelectron, respectively. $\mathrm{DAS}_i(\varepsilon_k)\times\exp\left(-\frac{t}{\tau_i}\right)$ is the contribution with a lifetime and amplitude of τ_i and $\mathrm{DAS}_i(\varepsilon_k)$, respectively. $H(t)$ is the unit step function. The corresponding (1+2') IRF is experimentally measured independently and described by a normalized Gaussian function. It should be clarified that a numerical convolution algorithm was employed here to calculate the result of $\left[\exp\left(-\frac{t}{\tau_i}\right) \times H(t)\right] \otimes$IRF, the intensity of which describes the detection efficiency of the excited state with a specific lifetime (τ_i) in a given time-resolved pump-probe measurement (a specific FWHM value of the IRF) [35]. Note that $\mathrm{DAS}_0(\varepsilon_k)\times$IRF represents the contribution from the two-color non-resonant photoionization signal, which is only around the time-zero. This component is weak compared with the resonant signal, but it cannot be totally neglected at pump wavelength of 259.5 nm (see FIG. S1 for details in Supplementary materials, SM) since the corresponding absorption cross section is very small. The component of IRF was also taken into account during the fit under similar situations in our previous time-resolved studies [10, 30, 31, 36].

A 2D global least-squares fit is achieved for the TRPES spectra at pump wavelengths of 259.5 and 238.6 nm. Three different time constants (τ_1, τ_2 and τ_3) together with their relative decay associated spectra (DAS) are obtained, as shown in FIG. 3 (a) and (b) for 259.5 and 238.6 nm respectively. The corresponding simulated 2D TRPES data are plotted in FIG. 3 (c) and (d). The time constants of 410±40 fs, 3.9±0.3 ps and 1.6±0.2 ns are derived at 259.5 nm. As the pump wavelength decreases to 238.6 nm, the time constants are 250±30 fs, 4.2±0.3 ps and 280±30 ps for τ_1, τ_2 and τ_3. In FIG. 4 (a) and (b), the normalized photoelectron transients derived by summing the TRPES data shown in FIG. 2 (a) and (b). The contributions of each component derived from the least-squares fit are also included. The initial decay of the transient is mainly described by the exponential decay associated with the time constant, τ_1, while the subsequent rise and decay signals at long delay times are totally fitted by the time constants, τ_2 and τ_3. The time constant of τ_1 should be assigned to the lifetime of the initially prepared excited state. The most important finding from the decay associated spectra is the result that $\mathrm{DAS}_2(\varepsilon_k)<0$ and $-\mathrm{DAS}_2(\varepsilon_k)\approx\mathrm{DAS}_3(\varepsilon_k)$ (see the inset of FIG. 3 (a, b)) in the whole photoelectron kinetic energy range. This indicates that the delayed rise signal is totally produced from the photoionization of a subsequently populated electronic state with an average lifetime of τ_3. At 218.3 nm, the TRPES spectrum actually has a poor sig-

DOI: 10.1063/1674-0068/cjcp2407099

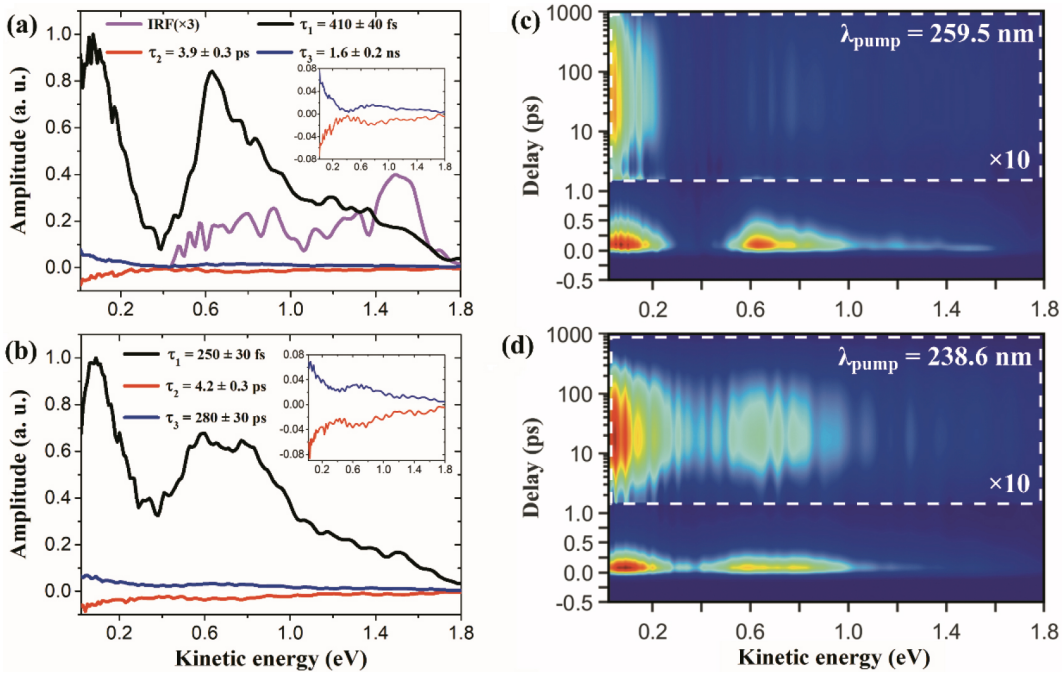

FIG. 3 (a, b) The photoelectron kinetic energy dependent amplitudes of each component (also called the decay associated spectra) derived from a 2D global least-squares fit to the TRPES data shown in FIG. 2(a, b), respectively. (c, d) The fit to the TRPES data shown in FIG. 2(a, b), respectively. It is simulated by using the derived time constants together with the decay associated spectra.

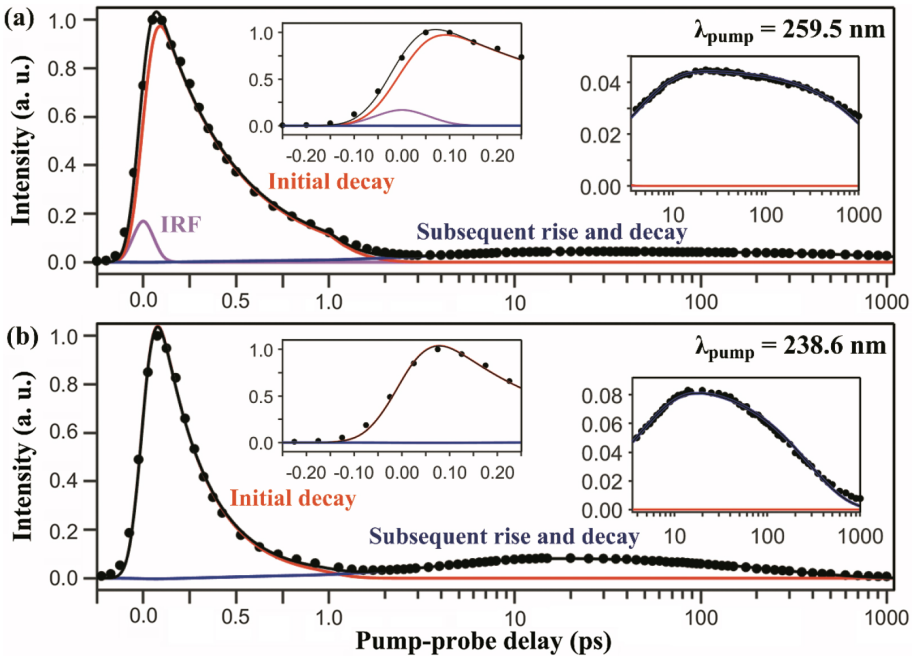

FIG. 4 (a, b) Normalized photoelectron transient derived by summing the TRPES data shown in FIG. 2(a, b), respectively. The contributions of each component (see text for details) derived from the least-squares fit are also included. The inset shows the transient in a specific delay range.

nal-to-noise ratio at delays of >1 ps. This drawback has prevented a reliable 2D global least-squares fit at long delay times and as such, the TRPES data are integrated over the whole kinetic energy range below 1.8 eV to derive a photoelectron transient. Then a least-squares fit to this transient is achieved and the corresponding time constants (τ_1, τ_2 and τ_3) are obtained (180±20 fs, 4.3±0.5 ps and 50±10 ps, see FIG. S2 in SM). All the derived time constants are summarized in Table I. In addition, a more detailed explanation about a multistep

DOI: 10.1063/1674-0068/cjcp2407099

TABLE I The pump wavelengths and the derived time constants.

λ_{pump}/nm	τ_1/fs	τ_2/ps	τ_3/ps
259.5	410±40	3.9±0.3	1600±300
238.6	250±30	4.2±0.3	280±30
218.3	180±20	4.3±0.5	50±10

sequential decay process is provided in SM. The assignment of the time constant of τ_2 is less clear-cut and will be further discussed in depth below in section III. C.

C. The excited-state decay dynamics

As we mentioned above, excitation at 259.5 and 238.6 nm pump wavelengths results in population of the first optically bright $S_2(^1\pi\pi^*)$ state, the lifetime of which is 410±40 fs at 259.5 nm and 250±30 fs at 238.6 nm. At 218.3 nm, there is no evidence in the TRPES spectrum that the $S_3(2^1\pi\pi^*)$ state starts to make a considerable contribution. Here we still assign the lifetime of 180±20 fs to the $S_2(^1\pi\pi^*)$ state with higher vibrational excitation. The delayed rise signal and the negative decay associated spectrum clearly indicates that a lower lying electronic state is subsequently populated. From a general point of view, the hot ground state even with large vibrational excess energy is not expected to be detectable under the probe conditions here since the Franck-Condon overlap between the ground state and the ionic manifold is rather poor.

Assuming this subsequently populated state which is associated with the delayed rise signal to be the $S_1(^1n\pi^*)$ state, the internal conversion process from the $S_2(^1\pi\pi^*)$ state to the $S_1(^1n\pi^*)$ state should happen and a time constant of about 4 ps is assigned to be associated with this decay path based on the analysis of our TRPES data. However, excited state population of the on-the-fly dynamics simulation indicated this time constant should be hundreds of femtoseconds in the case of 3-furfural [21], which is inconsistent with the above assumption. Moreover, it is not reasonable that both the time constants of τ_1 and τ_2 belong to the $S_2(^1\pi\pi^*)$ state when we consider the dramatic differences in the relative intensity and structure of the DAS_1 and DAS_2. In particular, the 2D global fitting result reveals that the absolute value of the DAS_2 (the negative one) associated with τ_2 is close to the value of the DAS_3 associated with τ_3 at all kinetic energies. This could not be rationalized within a simple two-step sequential decay process since three different time constants are needed in the fit and their DASs are broad over the whole kinetic energy range. Although there is a possibility that the relaxation out of the Franck-Condon region on the $S_2(^1\pi\pi^*)$ state potential energy surface is responsible for τ_1, while the lifetime of τ_2 is the further deactivation of the $S_2(^1\pi\pi^*)$ state minimum (*i.e.*, $^1\pi\pi^*_{FC}\rightarrow{}^1\pi\pi^*_{min}\rightarrow{}^1n\pi^*$). Meanwhile, in order to rationalize the fact that $-DAS_2(\varepsilon_k)\approx DAS_3(\varepsilon_k)$, the ionization cross section (σ_2) of the $S_2(^1\pi\pi^*)$ state minimum must be zero or at least much smaller than that (σ_3) of the subsequently populated $S_1(^1n\pi^*)$ state (see a sequential three-step kinetic model for more details in SM). This seems to be unreasonable since the $S_2(^1\pi\pi^*)$ state minimum should be effectively detected via two-photon ionization when the probe laser of 403.7 nm is employed here. Another alternative explanation is that the intramolecular vibrational energy redistribution (IVR) process of the subsequently populated $S_1(^1n\pi^*)$ state is responsible for τ_2, while the lifetime of τ_3 is the further deactivation of the $S_2(^1\pi\pi^*)$ state minimum (*i.e.*, $^1\pi\pi^*\rightarrow{}^1n\pi^*\rightarrow{}^1n\pi^*_{min}$). On the other hand, it is doubtful whether the time constant of τ_3 (*e.g.*, 1.6±0.2 ns at 259.5 nm) belongs to the $S_1(^1n\pi^*)$ state with large vibrational excess energy. At current pump wavelengths, the excitation energy is well above the S_1 origin of 3-furfural [33]. As a consequence, the $S_1(^1n\pi^*)$ state here is not expected to have such a long lifetime of τ_3. For example, in the case of acrolein, the lifetime of the $S_1(^1n\pi^*)$ state is several picoseconds [37, 38]. In future studies of 3-furfural, the dynamics of the $S_1(^1n\pi^*)$ state following direct photoexcitation may be observed by time-resolved experiments or the lifetime of the $S_1(^1n\pi^*)$ vibronic origin can be estimated from linewidth measurements. Then the above assignment of τ_2 and τ_3 can be more clearly ruled out if the measured lifetime of the directly excited $S_1(^1n\pi^*)$ state containing less vibrational energy (*e.g.*, the 0_0^0 band origin) is much smaller than the value of the time constant of τ_3.

As another possible explanation, we prefer to assign the time constant of τ_2 (~4 ps) to the lifetime of the $S_1(^1n\pi^*)$ state, while the lifetime of τ_3 (1.6±0.2 ns at 259.5 nm, 280±30 ps at 238.6 nm and 50±10 ps at 218.3 nm) is ascribed to the depopulation of a triplet state. This means that there exists a sequential three-step decay process, $S_2(^1\pi\pi^*)\rightarrow S_1(^1n\pi^*)\rightarrow T_n$. It is argued that an ultrafast intersystem crossing from the $S_1(^1n\pi^*)$ state to the triplet manifold can happen within the order of picosecond. We note that the value of

DOI: 10.1063/1674-0068/cjcp2407099

several picoseconds is suitable for intersystem crossing in some cases of typical linear/cyclic α,β-enones, such as acrolein [38], acetylacetone [39, 40], and 2-cyclopentenone [41]. The spin-orbit coupling between the $^1n\pi^*$ state and the energetically close-lying triplet state(s) was also discussed [41–43]. 3-Furfural can be regarded as one type of the cyclic α,β-enones. However, to the best of our knowledge, there has not yet been experimental evidence or calculation result to indicate that such ultrafast intersystem crossing occurs on a several picoseconds timescale for the decay of the $S_1(^1n\pi^*)$ state of 3-furfural. If this intersystem crossing process takes place in the case of 3-furfural, we propose that the subsequently populated triplet state is the $T_2(^3\pi\pi^*)$ state by considering the vertical energy of triplet states [25] and El-Sayed's rules [44]. The $T_2(^3\pi\pi^*)$ state and the $S_1(^1n\pi^*)$ state should prefer to yield an ionic ground state and an excited state, $D_0(\pi^{-1})$ and $D_1(n^{-1})$, respectively. This may explain why the ionization cross section (σ_2) of the $S_1(^1n\pi^*)$ state is much smaller than that (σ_3) of the $T_2(^3\pi\pi^*)$ state based on the result of our decay associated spectra (see details in SM). The unfavorable ionization cross section (σ_2) can be zero because the $S_1(^1n\pi^*)$ state at its minimum energy geometry seems to be energetically undetectable via two-photon ionization under the current probe conditions.

It should be clarified that only a fraction of the initially prepared wavepacket evolves on the $S_2(^1\pi\pi^*)$ state potential energy surface and decays to the $S_1(^1n\pi^*)$ state via internal conversion. The ring puckering pathway toward the ground state and the ring opening pathway via the $^1\pi\sigma^*$ state [21] are not monitored by the current probe laser of 403.7 nm (3.07 eV) since two-photon energy of 6.14 eV is insufficient for the photoionization of the vibrationally hot ground electronic state and the ring-opening intermediate(s). Therefore, these two relaxation pathways which also contribute to the lifetime of τ_1 (410±40 fs at 259.5 nm, 250±30 fs at 238.6 nm, and 180±20 fs at 218.3 nm) are not specifically discussed in the current study. The lifetime of the $S_2(^1\pi\pi^*)$ state is also pump wavelength-dependent based on our time-resolved pump-probe measurements, while the dynamics of the $S_2(^1\pi\pi^*)$ state at 267 nm has been reported previously by de Vivie-Riedle and coworkers [21]. The absolute branching ratios of these three decay channels are so far unknown. Here we tentatively suggest that the relaxation via the $^1n\pi^*$ state is a minor deactivation channel of the $S_2(^1\pi\pi^*)$ state. A future femtosecond time-resolved UV pump-VUV probe experiment is expected to provide a more complete picture of the excited-state dynamics of 3-furfural.

IV. CONCLUSION

In this paper, the UV photoinduced dynamics of 3-furfural upon excitation at pump wavelengths of 259.5, 238.6 and 218.3 nm is investigated using the TRPEI method. Excitation at these pump wavelengths results in population of the $S_2(^1\pi\pi^*)$ state, the lifetime of which is measured to be 410±40 fs at 259.5 nm, 250±30 fs at 238.6 nm and 180±20 fs at 218.3 nm. It is suggested that a fraction of the initially prepared wavepacket evolves out of the Franck-Condon region and funnels down to a local minimum on the multidimensional potential energy surface. Then further depopulation takes place with a lifetime of about 4 ps, resulting in the subsequent population of a lower lying state, the lifetime of which is in a range of 50 ps–1.6 ns. The picture of the excited-state dynamics of 3-furfural is far from complete. Further experimental investigations and theoretical calculations are expected to provide additional information and valuable insights to confirm the ambiguous interpretation about the delayed rise signal in the present experimental study.

Supplementary materials: The contribution of the two-color non-resonant signal at 259.5 nm, the fit to the photoelectron transient at 218.3 nm and a sequential three-step kinetic model are shown.

V. ACKNOWLEDGMENTS

This work was financially supported by the National Natural Science Foundation of China (No.22203095, No.22103087, and No.22288201), the State Key Laboratory of Molecular Reaction Dynamics (SKLMRD-Z202406) and the Chinese Academy of Sciences (GJJSTD20220001). We also gratefully acknowledge the support and assistance provided by the Dalian Coherent Light Source (DCLS).

[1] B. Marchetti, T. N. V. Karsili, M. N. R. Ashfold, and W. Domcke, Phys. Chem. Chem. Phys. **18**, 20007 (2016).
[2] S. Boldissar and M. S. de Vries, Phys. Chem. Chem. Phys. **20**, 9701 (2018).

[3] G. M. Roberts and V. G. Stavros, Chem. Sci. **5**, 1698 (2014).
[4] M. Filatov, S. Lee, H. Nakata, and C. H. Choi, Int. J. Mol. Sci. **22**, 4276 (2021).
[5] R. Uenishi, A. Boyer, S. Karashima, A. Humeniuk, and T. Suzuki, J. Phys. Chem. Lett. **15**, 2222 (2024).
[6] G. R. Wu, S. P. Neville, O. Schalk, T. Sekikawa, M. N. R. Ashfold, G. A. Worth, and A. Stolow, J. Chem. Phys. **142**, 074302 (2015).
[7] G. R. Wu, S. P. Neville, O. Schalk, T. Sekikawa, M. N. R. Ashfold, G. A. Worth, and A. Stolow, J. Chem. Phys. **144**, 014309 (2016).
[8] D. Y. Yang, Z. C. Chen, Z. G. He, H. D. Wang, Y. J. Min, K. J. Yuan, D. X. Dai, G. R. Wu, and X. M. Yang, Phys. Chem. Chem. Phys. **19**, 29146 (2017).
[9] D. Y. Yang, Y. J. Min, Z. C. Chen, Z. G. He, K. J. Yuan, D. X. Dai, X. M. Yang, and G. R. Wu, Phys. Chem. Chem. Phys. **20**, 15015 (2018).
[10] W. P. Yuan, D. Y. Yang, B. H. Feng, Y. J. Min, Z. C. Chen, S. R. Yu, G. R. Wu, and X. M. Yang, Phys. Chem. Chem. Phys. **23**, 17625 (2021).
[11] W. P. Yuan, B. H. Feng, D. Y. Yang, Y. J. Min, S. R. Yu, G. R. Wu, and X. M. Yang, Chin. J. Chem. Phys. **34**, 386 (2021).
[12] E. V. Gromov, A. B. Trofimov, F. Gatti, and H. Köppel, J. Chem. Phys. **133**, 164309 (2010).
[13] T. Fuji, Y. I. Suzuki, T. Horio, T. Suzuki, R. Mitrić, U. Werner, and V. Bonačić-Koutecký, J. Chem. Phys. **133**, 234303 (2010).
[14] M. Stenrup and Å. Larson, Chem. Phys. **379**, 6 (2011).
[15] A. Humeniuk, M. Wohlgemuth, T. Suzuki, and R. Mitrić, J. Chem. Phys. **139**, 134104 (2013).
[16] R. Spesyvtsev, T. Horio, Y. I. Suzuki, and T. Suzuki, J. Chem. Phys. **143**, 014302 (2015).
[17] D. M. P. Holland, E. A. Seddon, A. B. Trofimov, E. V. Gromov, M. Wormit, A. Dreuw, T. Korona, N. de Oliveira, L. E. Archer, and D. Joyeux, J. Mol. Spectrosc. **315**, 184 (2015).
[18] T. Petrenko and G. Rauhut, J. Chem. Phys. **148**, 054306 (2018).
[19] S. Adachi, T. Schatteburg, A. Humeniuk, R. Mitrić, and T. Suzuki, Phys. Chem. Chem. Phys. **21**, 13902 (2019).
[20] A. R. Smith and G. Meloni, J. Mass Spectrom. **50**, 1206 (2015).
[21] S. Oesterling, O. Schalk, T. Geng, R. D. Thomas, T. Hansson, and R. de Vivie-Riedle, Phys. Chem. Chem. Phys. **19**, 2025 (2017).
[22] M. Winfough, K. Voronova, G. Muller, G. Laguisma, B. Sztáray, A. Bodi, and G. Meloni, J. Phys. Chem. A **121**, 3401 (2017).
[23] A. Bhattacherjee, K. Schnorr, S. Oesterling, Z. Y. Yang, T. Xue, R. de Vivie-Riedle, and S. R. Leone, J. Am. Chem. Soc. **140**, 12538 (2018).
[24] O. Schalk, T. Geng, T. Hansson, and R. D. Thomas, J. Chem. Phys. **149**, 084303 (2018).
[25] N. Kuş, I. Reva, and R. Fausto, J. Phys. Chem. A **114**, 12427 (2010).
[26] C. Gregory and J. van Wijngaarden, J. Mol. Spectrosc. **373**, 111374 (2020).
[27] Z. G. He, Z. C. Chen, D. Y. Yang, D. X. Dai, G. R. Wu, and X. M. Yang, Chin. J. Chem. Phys. **30**, 247 (2017).
[28] Y. J. Min, W. P. Yuan, D. Y. Yang, D. X. Dai, S. R. Yu, G. R. Wu, and X. M. Yang, Chin. J. Chem. Phys. **35**, 242 (2022).
[29] D. Y. Yang, Y. J. Min, B. H. Feng, X. M. Yang, and G. R. Wu, Phys. Chem. Chem. Phys. **24**, 22710 (2022).
[30] B. H. Feng, D. Y. Yang, Y. J. Min, Q. H. Gao, B. J. Fang, G. R. Wu, and X. M. Yang, Phys. Chem. Chem. Phys. **25**, 17403 (2023).
[31] B. H. Feng, W. P. Wu, Z. G. He, D. Y. Yang, G. R. Wu, and X. M. Yang, J. Phys. Chem. A **128**, 3840 (2024).
[32] G. A. Garcia, L. Nahon, and I. Powis, Rev. Sci. Instrum. **75**, 4989 (2004).
[33] I. Colmenar, S. González, E. Jiménez, P. Martín, S. Salgado, B. Cabañas, and J. Albaladejo, Atmos. Environ. **103**, 1 (2015).
[34] T. Suzuki, L. Wang, and M. Tsubouchi, J. Phys. Chem. A **108**, 5764 (2004).
[35] B. H. Feng, W. P. Wu, S. K. Yang, Z. G. He, B. J. Fang, D. Y. Yang, G. R. Wu, and X. M. Yang, Phys. Chem. Chem. Phys. **26**, 8308 (2024).
[36] D. Y. Yang, Y. J. Min, Z. Chen, Z. G. He, Z. C. Chen, K. J. Yuan, D. X. Dai, G. R. Wu, and X. M. Yang, Chin. J. Chem. Phys. **32**, 53 (2019).
[37] K. W. Paulisse, T. O. Friday, M. L. Graske, and W. F. Polik, J. Chem. Phys. **113**, 184 (2000).
[38] Y. M. Wang, Z. F. Gu, L. Cao, B. Zhang, and S. Zhang, J. Phys. Chem. A **127**, 8595 (2023).
[39] A. Bhattacherjee, C. D. Pemmaraju, K. Schnorr, A. R. Attar, and S. R. Leone, J. Am. Chem. Soc. **139**, 16576 (2017).
[40] N. Kotsina, M. Candelaresi, L. Saalbach, M. M. Zawadzki, S. W. Crane, C. Sparling, and D. Townsend, Phys. Chem. Chem. Phys. **22**, 4647 (2020).
[41] O. Schalk, M. S. Schuurman, G. R. Wu, P. Lang, M. Mucke, R. Feifel, and A. Stolow, J. Phys. Chem. A **118**, 2279 (2014).
[42] G. L. Cui and W. Thiel, J. Chem. Phys. **141**, 124101 (2014).
[43] J. Cao and Z. Z. Xie, Phys. Chem. Chem. Phys. **18**, 6931 (2016).
[44] M. A. El-Sayed, J. Chem. Phys. **38**, 2834 (1963).

DOI: 10.1063/1674-0068/cjcp2407099